View metadata, citation and similar papers at
brought to you by CORE
provided by Digital.CSIC

PHYSICAL REVIEW B **88**, 081301(R) (2013)

Unoccupied topological surface state in Bi_2Te_2Se

Munisa Nurmamat,[1] E. E. Krasovskii,[2,3,4] K. Kuroda,[1] M. Ye,[5] K. Miyamoto,[6] M. Nakatake,[6] T. Okuda,[6] H. Namatame,[6] M. Taniguchi,[1,6] E. V. Chulkov,[2,3,7] K. A. Kokh,[8,9,10] O. E. Tereshchenko,[7,9,10] and A. Kimura[1,*]

[1]*Graduate School of Science, Hiroshima University, 1-3-1 Kagamiyama, Higashi-Hiroshima 739-8526, Japan*
[2]*Departamento de Física de Materiales UPV/EHU, CFM-MPC UPV/EHU, 20080 San Sebastián/Donostia, Basque Country, Spain*
[3]*Donostia International Physics Center (DIPC), 20018 San Sebastián/Donostia, Basque Country, Spain*
[4]*IKERBASQUE, Basque Foundation for Science, 48011 Bilbao, Spain*
[5]*Shanghai Institute of Microsystem and Information Technology, Chinese Academy of Sciences, Shanghai 200050, China*
[6]*Hiroshima Synchrotron Radiation Center, Hiroshima University, 2-313 Kagamiyama, Higashi-Hiroshima 739-0046, Japan*
[7]*Tomsk State University, Tomsk 634050, Russia*
[8]*V.S. Sobolev Institute of Geology and Mineralogy, Siberian Branch, Russian Academy of Sciences, Koptyuga pr. 3, Novosibirsk 630090, Russia*
[9]*A.V. Rzhanov Institute of Semiconductor Physics, Siberian Branch, Russian Academy of Sciences, pr. Akademika Lavrent'eva 13, Novosibirsk 630090, Russia*
[10]*Novosibirsk State University, ul. Pirogova 2, Novosibirsk 630090, Russia*

(Received 7 May 2013; published 5 August 2013)

Bias voltage dependent scattering of the topological surface state is studied by scanning tunneling microscopy/spectroscopy for a clean surface of the topological insulator Bi_2Te_2Se. A strong warping of constant energy contours in the unoccupied part of the spectrum is found to lead to a spin-selective scattering. The topological surface state persists to higher energies in the unoccupied range far beyond the Dirac point, where it coexists with the bulk conduction band. This finding sheds light on the spin and charge dynamics over a wide energy range and opens a way to designing optospintronic devices.

DOI: 10.1103/PhysRevB.88.081301 PACS number(s): 73.20.−r, 71.20.Nr, 72.10.Fk

Three-dimensional topological insulators (3D TIs) represent a recently discovered state of matter, whose hallmark is the surface state in the absolute bulk energy gap, which has a spin nondegenerate Dirac-cone energy dispersion and helical spin texture.[1–6] The topological surface state (TSS) is protected by time-reversal symmetry and is robust against nonmagnetic perturbations.

Of all the 3D TIs, the most extensively studied is Bi_2Se_3 owing to its large energy gap and the single TSS.[7,8] However, in spite of significant efforts to realize the surface isolated transport in Bi_2Se_3, the progress has been hampered by a too small surface contribution to the total conductance compared to the uncontrolled bulk contribution from the carrier doping due to the Se vacancies.[9,10]

Here we focus on Bi_2Te_2Se, which has been theoretically predicted to be a 3D TI (Ref. 11), and this was confirmed by angle-resolved photoemission spectroscopy (ARPES).[12–14] A highly spin polarized TSS in Bi_2Te_2Se has been observed in recent spin-resolved ARPES (SARPES) measurements.[15] Bi_2Te_2Se has an ordered tetradymite structure, derived from Bi_2Te_3 by replacing the central Te layer with a Se layer. Because here the Se atoms are confined in the central layer the formation of Se vacancies and the antisite defects between Bi and Te atoms is expected to be less probable,[16] which would suppress the bulk conductivity. Indeed, this compound has been found to be bulk insulating, and surface-derived quantum oscillations have been observed in a magnetotransport experiment.[16] This makes Bi_2Te_2Se very promising for spintronic applications.

Interband optical excitation of topological surface states by pulsed laser light is expected to generate longer-lived spin-polarized carriers at the surface.[17,18] To understand the photoexcited spin and charge dynamics, knowledge of the unoccupied topological surface state far above the Dirac point and the unoccupied bulk continuum is crucial. Note that photoelectron spectroscopy, with which most of the studies on topological insulators have been performed, cannot access unoccupied states or provide direct information on the in-plane electron scattering. Thus, there has been a dearth of measurements on the unoccupied electronic states of 3D TIs, and the present study is motivated by the necessity of getting the information about the unoccupied spectrum.

Scanning tunneling microscopy (STM)/spectroscopy (STS) has been widely used to study the surfaces of 3D TIs as the most surface sensitive technique providing direct information on the electronic structure of topological surface states and their scattering properties. One can unveil the spin structure of surface states through the presence or absence of standing waves both for occupied and unoccupied states. Fourier transformed images of the observed standing waves give bias-dependent scattering vectors in momentum space. For an isotropic TSS, the backscattering is strongly suppressed, while a spin-conserving scattering is allowed, and it has actually been observed in several topological insulators with warped constant energy contours (CECs).[19–26] A non-spin-conserving scattering can also occur if the time reversal symmetry is broken, i.e., in the presence of magnetic impurities.[27]

In this Rapid Communication, a quasiparticle interference pattern due to surface scattering is revealed on Bi_2Te_2Se with a low-temperature STM (LT-STM) experiment over a wide sample bias energy range. A strong warping of CECs of the TSS explains the anisotropic spin-conserving scattering, which persists into the unoccupied state region, where the surface state coexists with the bulk conduction band.

 ©2013 American Physical Society

Our experiments were performed using an LT-STM (Omicron NanoTechnology GmbH) operated at 4.5 K in an ultrahigh vacuum. The Bi_2Te_2Se crystal was grown by the modified vertical Bridgman method as described elsewhere.[28] The STM images were obtained in a constant-current mode, and the differential conductance dI/dV maps were measured simultaneously with recording the STM images using a standard lock-in technique. ARPES experiments were conducted using the synchrotron radiation at the beamline (BL-7) equipped with a hemispherical photoelectron analyzer (VG-SCIENTA SES2002) of the Hiroshima Synchrotron Radiation Center (HSRC). Samples were cleaved in an ultrahigh vacuum *in situ* at room temperature for the STM and at 10 to 20 K for ARPES measurement.

Similar to Bi_2Se_3 and Bi_2Te_3, Bi_2Te_2Se forms a rhombohedral crystal structure with the space group D^5_{3d} ($R\bar{3}m$), with the basis quintuple layer (QL) unit of Te-Bi-Se-Bi-Te, as depicted in Fig. 1(a). Inside the QL the bonds are predominantly ionic covalent, and adjacent QLs are bound by van der Waals forces. Figure 1(b) is the atomic-resolution image (−50 mV, 0.12 nA) of the Bi_2Te_2Se surface area of 5 nm × 5 nm. The scanning tunneling spectrum gives a measure of the local density of states near the Fermi energy as shown in Fig. 1(c). The resulting STS data were averaged over 10 spectra to improve the statistics. The dashed lines show approximate energy locations of the top of the bulk valence band (BVB), the Dirac point (DP), and the bottom of the bulk conduction band (BCB) around the $\bar{\Gamma}$ point. Figure 1(d) depicts the surface state energy dispersion of Bi_2Te_2Se measured by ARPES at the photon energy of $h\nu = 30$ eV [open circles indicate the band dispersion by our *ab initio* calculation (see Fig. 3) shifted downward by 0.24 eV to match the measured Dirac point position]. The DP energies from ARPES and STS spectra are equal.[29]

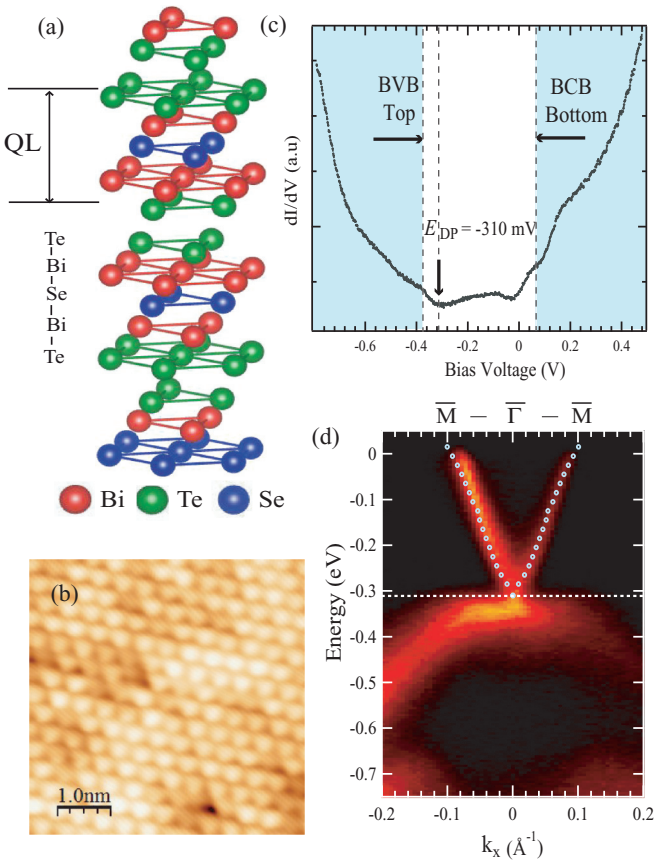

FIG. 1. (Color online) (a) Crystal structure showing three quintuple units of Bi_2Te_2Se. (b) The atomic-resolution image (5 nm × 5 nm) on the surface of Bi_2Te_2Se obtained with a bias voltage of −50 mV. (c) Averaged STS spectrum indicating the approximate position for the Dirac point (E_{DP}), top of the bulk valence band (E_{BVB}), and bottom of the bulk conduction band (E_{BCB}). (d) Energy-momentum ARPES intensity distribution map along the $\bar{\Gamma}\bar{M}$ direction for the photon energy of 30 eV.

Figure 2(a) shows the differential conductance (dI/dV) map at a bias voltage of $V_s = +750$ mV. It exhibits a standing wave spreading anisotropically around point defects. (All the spectroscopic maps at the bias voltages from +50 to +1250 mV were obtained for the same surface without changing any other experimental parameters.) In order to get the momentum space information and obtain the scattering wave vectors, we have performed a fast Fourier transformation (FFT) of the dI/dV maps; see Figs. 2(b)–2(l). These scattering images provide information on bias-dependent quasiparticle interference. For bias voltages below +300 mV the interference effect around the point defects is weak, and the FFT image shows a circular pattern with small $\mathbf{q}$ vectors, which mainly come from the statistical noise. At $V_s = +400$ mV, flower shaped patterns emerge [Fig. 2(b)] with six broad petals along $\bar{\Gamma}\bar{M}$. Note that the pattern becomes sharp and intensive at bias voltages between +550 and +850 mV. Starting with $V_s = +950$ mV, with increasing the bias voltage the spots get gradually broader.

The evolution of the scattering vectors with V_s is visualized by the FFT power profiles in Figs. 2(m) and 2(n). In Fig. 2(m), in the $\bar{\Gamma}\bar{M}$ direction (rightwards) the scattering vectors become larger as V_s increases, while there is practically no scattering along $\bar{\Gamma}\bar{K}$ (leftwards). In Fig. 2(n) we show the ratio of the intensity profiles along $\bar{\Gamma}\bar{M}$ and $\bar{\Gamma}\bar{K}$. The intensities ratio damps the background and makes the scattering more clear: we distinctly see the dispersion of q with the bias voltage.

In order to elucidate the origin of scattering pattern and the effect of the helical spin texture of the TSS, we have performed a first-principles calculation of the electronic structure of a seven formula units slab of Bi_2Te_2Se (Ref. 30). Figure 3(a) shows the band structure along $\bar{\Gamma}\bar{K}$ (leftwards) and $\bar{\Gamma}\bar{M}$ (rightwards). The magenta arrows show the energy and momentum ranges of the TSS, and the green arrows indicate the range of the inner surface state (ISS), which splits off from the top of the conduction band. Here, the DP is localized 0.065 eV below the calculated Fermi energy, i.e., the experimental energy scale is shifted by 0.24 eV relative to the theoretical scale. Figures 3(b) and 3(c) show the depth-momentum distribution (in the $\bar{\Gamma}\bar{K}$ direction) of the charge density $\rho(z,k_\parallel)$ for the upper-cone TSS [Fig. 3(b)] and for the ISS [Fig. 3(c)]. The upper-cone surface state exists up to $k_\parallel = 0.22$ Å^{-1}, and the ISS between 0.08 and 0.2 Å^{-1}.

Figures 3(d)–3(f) show calculated momentum distributions of the spatially resolved spectral density $N(E,\mathbf{k}_\parallel)$ at three constant energies E. The function is defined as a sum over all (discrete) states λ with energy E and Bloch vector $\mathbf{k}_\parallel$ weighted with the probability $Q_{\lambda\mathbf{k}_\parallel}$ of finding the electron in this state in the surface region: $N(E,\mathbf{k}_\parallel) = \sum_\lambda Q_{\lambda\mathbf{k}_\parallel}\delta(E_{\lambda\mathbf{k}_\parallel} - E)$.

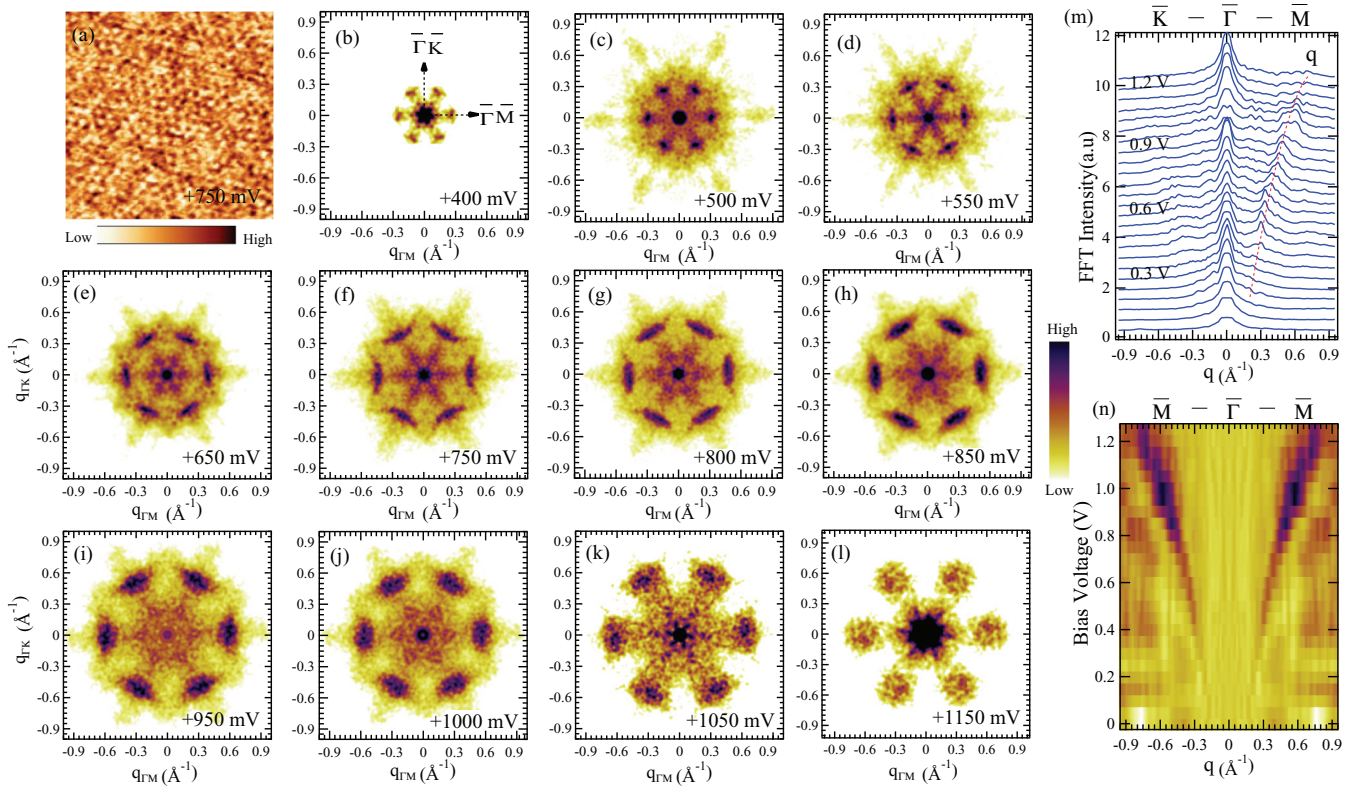

FIG. 2. (Color online) (a) Differential conductance map (dI/dV map) of Bi_2Te_2Se surface at 4.5 K with a sample bias voltage of 750 mV in the 45 nm × 45 nm area (set point $I = 0.15$ nA). (b)–(l) Fast Fourier transformed images for several bias voltages showing six strong spots along the $\bar{\Gamma}\bar{M}$ direction. The FFT patterns are hexagonally symmetrized. (m) FFT intensity profiles from +0.05 V to +1.25 V with a step of +0.05 V display the bias voltage dependent scattering along the $\bar{\Gamma}\bar{M}$ (positive q) and $\bar{\Gamma}\bar{K}$ (negative q) directions. (n) The ratio of the FFT intensity profiles along $\bar{\Gamma}\bar{M}$ and $\bar{\Gamma}\bar{K}$.

(For the sake of presentation, the δ function is replaced by a Gaussian of 0.05 eV full width at half maximum.) The integral $Q_{\lambda\mathbf{k}_\parallel} = \int |\psi_{\lambda\mathbf{k}_\parallel}(\mathbf{r})|^2 d\mathbf{r}$ over the surface region comprises two outermost atomic layers and vacuum.

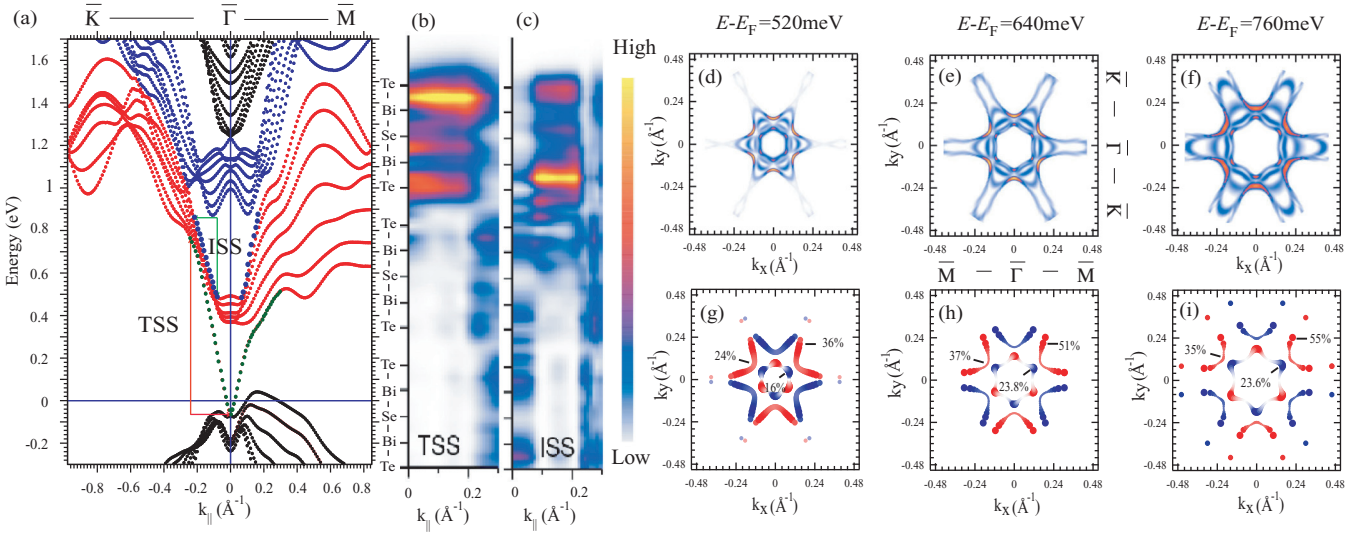

FIG. 3. (Color online) (a) First-principles electronic structure of a seven formula units slab of Bi_2Te_2Se. (b), (c) The depth-momentum distribution of the charge density for the TSS and ISS. Because of the finite thickness of the slab we show the sum of densities of the degenerate pair of the surface states located on the opposite surfaces of the slab. (d)–(f) Spatially resolved Fermi surfaces. The color scale shows the constant energy cuts of the surface spectral function $N(z,k_\parallel)$. (g)–(i) Distribution of the spin polarization perpendicular to the surface; red and blue circles denote positive and negative spin polarization, and their sizes represent the magnitudes of spin polarization. The spin polarization values are shown at some specific points.

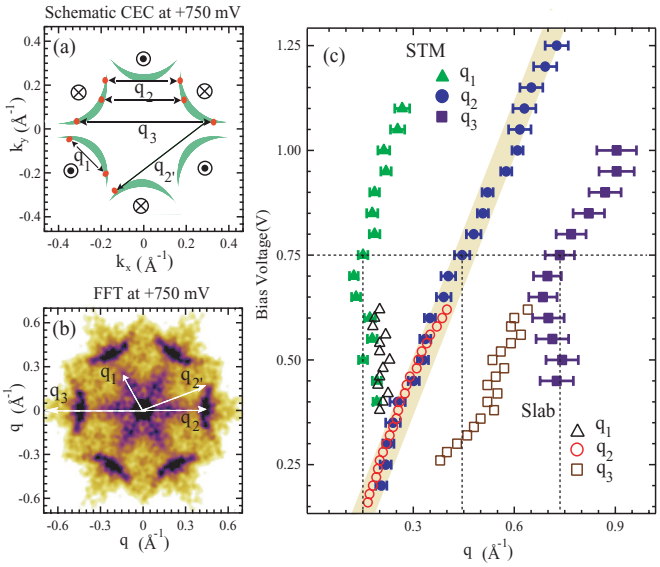

FIG. 4. (Color online) (a) Schematic CEC with possible scattering vectors and (b) experimental FFT image at a bias voltage of +750 mV. The $\bar{\Gamma}\bar{M}$ direction is along the x axis. (c) Dispersion of three scattering vectors from STM (filled symbols) and the slab calculation (open symbols).

The angular distribution of the spin polarization perpendicular to the surface for the two surface states, TSS and ISS, is shown in Figs. 3(g)–3(i). Here the net spin density is integrated over a half of the slab, and the net spin is normalized to the electron charge in the integration region.

The TSS is somewhat stronger localized than the ISS [cf. Figs. 3(b) and 3(c)], and it exhibits a higher out-of-plane spin polarization. It is most interesting that the magnitude of the out-of-plane spin polarization of the TSS may be as large as 55%.

The bias-dependent quasiparticle scattering is characterized by scattering vectors that connect the **k** vectors of the initial and final scattering states at the CEC. Figure 4(a) shows schematic CEC of the TSS. Three characteristic scattering vectors denoted as $\mathbf{q}_1$, $\mathbf{q}_2$, and $\mathbf{q}_3$ explain the features in Fig. 4(b). The most intense croissant-shaped features can only be explained by $\mathbf{q}_2$ and $\mathbf{q}_2'$, which connect two flat segments of the contour as shown in Fig. 4(a). Other scattering features along the $\bar{\Gamma}\bar{M}$ direction characterized by $\mathbf{q}_1$ and $\mathbf{q}_3$ can also be explained as due to the warping of the TSS. The scattering originating from the ISS can be excluded because its CEC has no parallel fragments to cause a large joint density of states, and its convex shape does not lead to the croissant-shaped structures.

To clarify the relation between experimental and theoretical results, the intensity maxima of the FFT power profiles in the $\bar{\Gamma}\bar{M}$ direction in Fig. 2(m) are compared with the q values extracted from the slab calculation; see Fig. 4(c). By shifting the calculated points upward by 0.1 eV we were able to reproduce all the experimentally observed scattering features. (A discrepancy of the same order between the two photon photoemission measurements of the unoccupied Dirac cone and calculations was reported in Ref. 12.)

The presence of the FFT features in the $\bar{\Gamma}\bar{M}$ direction and their absence in the $\bar{\Gamma}\bar{K}$ direction tells us that the scattering is strongly spin selective. This scattering scenario holds for the whole energy interval from +300 to +1000 mV above the Fermi energy, and no significant surface to bulk scattering is observed, in contrast to Bi_2Se_3, for which a bulk-related scattering has been reported.[23] This indicates that a coupling of the TSS with the bulk continuum states is negligible even in the unoccupied region, which energetically overlaps with the bulk conduction band.

In conclusion, our scanning tunneling microscopy/spectroscopy experiment and the first-principles calculation of Bi_2Te_2Se reveal a scattering pattern that originates from the strongly warped constant energy contours of the topological surface state with substantial out-of-plane spin polarization. The topological surface state is thus found to survive up to energies far above the Dirac point. This unusual persistence of a Dirac surface state with spin texture provides a deeper understanding of optically excited spin and charge dynamics at the surface of topological insulators by pulsed laser light, which could be harnessed for optospintronic devices.

STM and ARPES measurements were performed with the approval of the Proposal Assessing Committee of HSRC (Proposals No. 11-B-40 and No. 10-A-32). This work was financially supported by KAKENHI (Grants No. 20340092 and No. 23340105), a Grant-in-Aid for Scientific Research (B) of JSPS, and RFBR Research Project No. 13-02-92105 a. The authors acknowledge partial support from the Spanish Ministerio de Ciencia e Innovación (Grant No. FIS2010-19609-C02-02).

*akiok@hiroshima-u.ac.jp

[1] M. Z. Hasan and C. L. Kane, Rev. Mod. Phys. **82**, 3045 (2010).
[2] J. E. Moore, Nature (London) **464**, 194 (2010).
[3] L. Fu, C. L. Kane, and E. J. Mele, Phys. Rev. Lett. **98**, 106803 (2007).
[4] X. L. Qi and S. C. Zhang, Rev. Mod. Phys. **83**, 1057 (2011).
[5] M. Z. Hasan and J. E. Moore, Annu. Rev. Conds. Matter Phys. **2**, 55 (2011).
[6] T. Okuda and A. Kimura, J. Phys. Soc. Jpn. **82**, 021002 (2013).
[7] Y. Xia, D. Qian, D. Hsieh, L. Wray, A. Pal, H. Lin, A. Bansil, D. Grauer, Y. S. Hor, R. J. Cava, and M. Z. Hasan, Nat. Phys. **5**, 398 (2009).
[8] K. Kuroda, M. Arita, K. Miyamoto, M. Ye, J. Jiang, A. Kimura, E. E. Krasovskii, E. V. Chulkov, H. Iwasawa, T. Okuda, K. Shimada, Y. Ueda, H. Namatame, and M. Taniguchi, Phys. Rev. Lett. **105**, 076802 (2010).
[9] N. P. Butch, K. Kirshenbaum, P. Syers, A. B. Sushkov, G. S. Jenkins, H. D. Drew, and J. Paglione, Phys. Rev. B **81**, 241301(R) (2010).

[10]K. Eto, Z. Ren, A. A. Taskin, K. Segawa, and Y. Ando, Phys. Rev. B **81**, 195309 (2010).

[11]L. L. Wang and D. D. Johnson, Phys. Rev. B **83**, 241309(R) (2011).

[12]T. Arakane, T. Sato, S. Souma, K. Kosaka, K. Nakayama, M. Komatsu, T. Takahashi, Z. Ren, K. Segawa, and Y. Ando, Nat. Comms. **3**, 636 (2012).

[13]M. Neupane, S.-Y. Xu, L. A. Wray, A. Petersen, R. Shankar, N. Alidoust, C. Liu, A. Fedorov, H. Ji, J. M. Allred, Y. S. Hor, T. R. Chang, H. T. Jeng, H. Lin, A. Bansil, R. J. Cava, and M. Z. Hasan, Phys. Rev. B **85**, 235406 (2012).

[14]D. Niesner, Th. Fauster, S. V. Eremeev, T. V. Menshchikova, Yu. M. Koroteev, A. P. Protogenov, E. V. Chulkov, O. E. Tereshchenko, K. A. Kokh, O. Alekperov, A. Nadjafov, and N. Mamedov, Phys. Rev. B **86**, 205403 (2012).

[15]K. Miyamoto, A. Kimura, T. Okuda, H. Miyahara, K. Kuroda, H. Namatame, M. Taniguchi, S. V. Eremeev, T. V. Menshchikova, E. V. Chulkov, K. A. Kokh, and O. E. Tereshchenko, Phys. Rev. Lett. **109**, 166802 (2012).

[16]Z. Ren, A. A. Taskin, S. Sasaki, K. Segawa, and Y. Ando, Phys. Rev. B **82**, 241306(R) (2010).

[17]P. Hosur, Phys. Rev. B **83**, 035309 (2011).

[18]J. A. Sobota, S. Yang, J. G. Analytis, Y. L. Chen, I. R. Fisher, P. S. Kirchmann, and Z. X. Shen, Phys. Rev. Lett. **108**, 117403 (2012).

[19]T. Zhang, P. Cheng, X. Chen, J. F. Jia, X. C. Ma, K. He, L. L. Wang, H. J. Zhang, X. Dai, Z. Fang, X. C. Xie, and Q. K. Xue, Phys. Rev. Lett. **103**, 266803 (2009).

[20]L. Fu, Phys. Rev. Lett. **103**, 266801 (2009).

[21]P. Roushan, J. Seo, C. V. Parker, Y. S. Hor, D. Hsieh, D. Qian, A. Richardella, M. Z. Hasan, R. J. Cava, and A. Yazdani, Nature (London) **460**, 1106 (2009).

[22]Z. Alpichshev, J. G. Analytis, J. H. Chu, I. R. Fisher, Y. L. Chen, Z. X. Shen, A. Fang, and A. Kapitulnik, Phys. Rev. Lett. **104**, 016401 (2010).

[23]S. Kim, M. Ye, K. Kuroda, Y. Yamada, E. E. Krasovskii, E. V. Chulkov, K. Miyamoto, M. Nakatake, T. Okuda, Y. Ueda, K. Shimada, H. Namatame, M. Taniguchi, and A. Kimura, Phys. Rev. Lett. **107**, 056803 (2011).

[24]H. Beidenkopf, P. Roushan, J. Seo, L. Gorman, I. Drozdov, Y. S. Hor, R. J. Cava, and A. Yazdani, Nat. Phys. **7**, 939 (2011).

[25]Z. Alpichshev, R. R. Biswas, A. V. Balatsky, J. G. Analytis, J. H. Chu, I. R. Fisher, and A. Kapitulnik, Phys. Rev. Lett. **108**, 206402 (2012).

[26]M. Ye, S. V. Eremeev, K. Kuroda, E. E. Krasovskii, E. V. Chulkov, Y. Takeda, Y. Saitoh, K. Okamoto, S. Y. Zhu, K. Miyamoto, M. Arita, M. Nakatake, T. Okuda, Y. Ueda, K. Shimada, H. Namatame, M. Taniguchi, and A. Kimura, Phys. Rev. B **85**, 205317 (2012).

[27]Y. Okada, C. Dhital, W. W. Zhou, E. D. Huemiller, H. Lin, S. Basak, A. Bansil, Y. B. Huang, H. Ding, Z. Wang, S. D. Wilson, and V. Madhavan, Phys. Rev. Lett. **106**, 206805 (2011).

[28]K. A. Kokh, B. G. Nenashev, A. E. Kokh, and G. Y. Shvedenkov, J. Cryst. Growth **275**, e2129 (2005).

[29]S. Jia, H. Beidenkopf, I. Drozdov, M. K. Fuccillo, J. Seo, J. Xiong, N. P. Ong, A. Yazdani, and R. J. Cava, Phys. Rev. B **86**, 165119 (2012).

[30]Self-consistent calculations within the local density approximation were performed with the full-potential augmented plane wave method described in E. E. Krasovskii, F. Starrost, and W. Schattke, Phys. Rev. B **59**, 10504 (1999).